Partial integration of ADM1 into CFD: understanding the impact of diffusion on anaerobic digestion mixing

Yohannis Mitiku Tobo IWA, Usman Rehman IWA, Jan Bartacek IWA and Ingmar Nopens IWA

ABSTRACT

Sufficient mixing is crucial for the proper performance of anaerobic digestion (AD), creating a homogeneous distribution of soluble substrates, biomass, pH, and temperature. The opaqueness of the sludge and mode of operation make it challenging to study AD mixing experimentally. Therefore, hydrodynamics modelling employing computational fluid dynamics (CFD) is often used to investigate this mixing. However, CFD models mostly do not include biochemical reactions and, hence, ignore the effect of diffusion-induced transport on AD heterogeneity. The novelty of this work is the partial integration of Anaerobic Digestion Model no. 1 (ADM1) into the CFD model. The aim is to better understand the effect of advection–diffusion transport on the homogenization of soluble substrates and biomass. Furthermore, AD homogeneity analysis in terms of concentration distribution is proposed rather than the traditional velocity distributions. The computed results indicate that including diffusion-induced transport affects the homogeneity of AD.

Key words | ADM1, advection–diffusion, CFD model, concentration, Peclet number, Schmidt number

Yohannis Mitiku Tobo IWA (corresponding author)
Ingmar Nopens IWA
BIOMATH, Department of Data Analysis and Mathematical Modelling,
Ghent University,
Coupure Links 653, B-9000 Ghent,
Belgium
E-mail: yohannismitiku.tobo@ugent.be

Yohannis Mitiku Tobo
Jan Bartacek IWA
Department of Water Technology and Environmental Engineering,
University of Chemistry and Technology Prague,
Technicka 5, 166 28 Prague 6,
Czech Republic

Usman Rehman IWA
AM-TEAM,
Oktrooiplein 1- Box 601, 9000 Ghent,
Belgium

INTRODUCTION

Generally, it is assumed that mixing enhances the performance of anaerobic digestion (AD), creating a homogeneous distribution of soluble substrates, biomass, pH, and temperature. The reported computational fluid dynamics (CFD) models of mechanically agitated anaerobic digesters mostly dealt solely with hydrodynamics. They focused on understanding the effects of sludge rheology, impeller speed, turbulence model selection, geometric configuration, analysis of flow field and evaluation of dead volume for scale-down, laboratory, and pilot-scale anaerobic digesters (Wu & Chen 2008; Meroney & Colorado 2009; Wu 2010; Yu et al. 2011; Bridgeman 2012; Craig et al. 2013; Leonzio 2018; Wiedemann et al. 2018; Conti et al. 2019).

After the development of Anaerobic Digestion Model no. 1 (ADM1) by the International Water Association (IWA) task group, several slight modifications have been formulated and applied in kinetics modelling while little effort has been made to integrate the kinetic model into the CFD model. For example, Wu (2012) modelled an integrated mixing, heat transfer, and fermentation of an egg-shaped anaerobic digester, and showed the distribution of biomass, pH, temperature, mixing, and heat transfer affect methane yield. Gaden & Bibeau (2013) and Rezavand et al. (2019) suggested the implementation of ADM1 into the CFD model, but the stiffness of the kinetic model and solver efficiency proved to be challenging to apply the CFD-kinetic modelling extensively. Other authors like Donoso-Bravo et al. (2018) proposed the integration of ADM1 into a compartmental model intending to understand the spatial variation of soluble substrates, biomass, and pH.

The findings of the AD CFD model hydrodynamics in the literature show that the velocity distribution decreases with increasing total suspended solids (TSS), hence reducing system performance. However, data collected from 2015 to 2017 from a full-scale anaerobic digester in Breda, The Netherlands, indicate that the digester was normally operating at sludge TSS ranging from 3 to 10% and at constant

mixing speed. These two contradicting cases suggest that there are knowledge gaps in currently used models that study AD mixing. We hypothesize that the CFD hydrodynamic models alone cannot predict the mixing of AD accurately since the effects of (molecular and turbulent) diffusion and biogas bubbles are ignored. Moreover, velocity is not a good descriptor of mixing homogeneity since minimum velocity required to produce uniform mixing is still unknown. Understanding the effect of diffusion-induced transport on AD mixing and describing the homogeneity of AD in terms of concentration distribution are hence the aim of this work.

METHODS

This work has two sections. The first section deals with the CFD hydrodynamics modelling of AD. In this section, the homogeneity of AD mixing is described based on velocity distribution. Subsequently, user defined scalar (UDS) transport equations are implemented over the converged and frozen hydrodynamic model in the second section. Part of the ADM1 model is implemented as UDS to simulate concentrations and to allow the effect of diffusion-induced transport to be included. We restricted this to hydrolysis of carbohydrate, protein, and lipids to soluble sugar, amino acids, and long-chain fatty acids (LCFAs), respectively, and growth of biomass, which degrades the hydrolysis products.

GEOMETRY, MESH AND HYDRODYNAMICS MODELLING

The anaerobic digester under study is located in Breda, The Netherlands, and has a volume of 9,000 m^3, two stage mixers with three hydrofoil type impellers on each stage, and operates at TSS of 3–10%. The digester was scaled down by the ratio of 1–20 to reduce the computational burden. Figure 1 (left) shows the scaled-down geometry and its detailed dimensions.

A multiple reference frame is selected to implement the flow feature of the impeller rotation. A rotating reference frame (RRF) for each stage of the impellers and a stationary reference frame are created. The impellers are enclosed in an RRF and connected to the stationary reference frame using an interface boundary condition.

The stationary and rotating reference frames are meshed by a sweeping method for sweepable bodies and hex-dominant for non-sweepable bodies. The mesh independence test runs for three different mesh sizes consisting of 1.2, 1.6, and 3.2 million elements. Figure 1 (right) shows the final mesh with 3.2 million cells, for which the simulation proved to be independent of mesh size.

In this work, 4% of TSS sludge is considered to study the impact of diffusion-induced transport. The occurrence of density gradients due to digested sludge sedimentation is expected to be very low. For this reason, as well as to avoid the complexity of a multiphase model introducing many additional empirical parameters to describe the momentum transfer between the phases, simulating the system as a single-phase fluid is reasonable. The free surface at the top of the digester is ignored and treated as a wall boundary condition. An inlet velocity is defined at the inlet of the digester (Figure 1). Since the details of the flow velocity and pressure are not known before solving the flow problem, the outflow boundary condition is defined at the outlet. The hydrodynamics of AD mixing is solved, treating the sludge rheology as non-Newtonian fluid, employing a Herschel–Bulkley rheology model and k-ε turbulence model. The rotational speed of both mixers is set to 50 rpm.
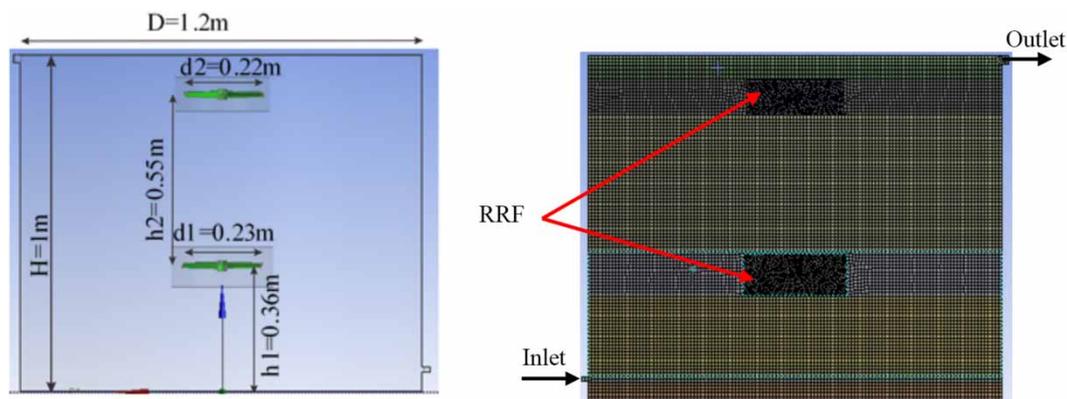

Figure 1 | Schematic drawing of scaled-down anaerobic digester (left) and a sectional view of meshed anaerobic digester geometry (right).

GOVERNING EQUATIONS OF UDS TRANSPORT MODELLING

The UDS transport equations are solved after the hydrodynamics simulation has converged. Continuity, momentum, and turbulence modelling equations are disabled (frozen) before implementing and solving the UDS transport equations. Activating the source term in Ansys Fluent enables the advection–diffusion Equation (1) with diffusion transport or Equation (2) without diffusion transport for steady state simulation.

$$\frac{\partial}{\partial x_i}\left(\rho u_i \phi_k - \Gamma_{eff}\frac{\partial \phi_k}{\partial x_i}\right) = S_{\phi_k} \tag{1}$$

$$\frac{\partial}{\partial x_i}(\rho u_i \phi_k) = S_{\phi_k} \tag{2}$$

where x_i is the position, u_i is the velocity, ϕ_k is the scalar variable, $k = 1, 2,..., N$. S_{ϕ_k} is the source term, ρ is the sludge density and Γ_{eff} is the effective (molecular and turbulent) diffusion coefficient (Equation (3)).

$$\Gamma_{eff} = \rho D_{i,lam} + \frac{\mu_t}{Sc_t} \tag{3}$$

where $D_{i,lam}$ is the molecular diffusion coefficient. Due to a lack of substrates and biomass diffusion coefficients for sludge, $D_{i,lam}$ of glucose in an alginate gel solution, $6.4 \times 10^{-10}\,\text{m}^2/\text{s}$, is adopted for all substrates (Øyaas *et al.* 1995). Furthermore, a bacteria diffusion coefficient of $2.8 \times 10^{-11}\,\text{m}^2/\text{s}$ is adopted for all biomass (Douarche *et al.* 2009) and μ_t represents the turbulent viscosity (Equation (4)).

$$\mu_t = \rho C_\mu \frac{k^2}{\varepsilon} \tag{4}$$

where k is the turbulent kinetic energy, ε is the eddy dissipation and the details of C_μ are found in Ansys (2009). Sc_t is the turbulent Schmidt number, which is an empirical constant and relatively insensitive to the fluid properties. Sc_t is the ratio of turbulent momentum diffusivity (eddy viscosity), v_t, to mass diffusivity, D_t (Equation (5).

$$Sc_t = \frac{v_t}{D_t} \tag{5}$$

Usually, the value of Sc_t is between 0.5 and 0.9 (Tominaga & Stathopoulos 2007). The effect of turbulent diffusion on AD mixing is analyzed for Sc_t values, i.e. 0.5, 0.7, and 0.9.

Introducing the non-dimensionless Peclet (Pe) number (Equation (6)) helps to describe advection–diffusion transport clearly. Pe is the ratio of advection transport to diffusion transport. In regions where Pe < 1, diffusion transport is dominant while in regions with Pe > 1, advection transport is dominant (Ghatak 2016).

$$Pe = \frac{ud}{D} \tag{6}$$

where u is the flow velocity, d is the characteristic length and D is the molecular diffusion coefficient of soluble substrates.

ADM1 EQUATIONS IMPLEMENTED INTO CFD MODEL

The scalar variable (ϕ_k) in Equations (1) and (2) results from either hydrolysis (Equation (7)) or growth of biomass on soluble substrates (Equation (8)). Three hydrolysis products, three biomass growth, and two diffusion equations, as well as three initial conditions are written in C and compiled into Ansys Fluent 19 R1.

The first-order rate Equation (7) represents the hydrolysis of carbohydrates, lipids, and proteins to their respective soluble substrate.

$$\frac{dS_j}{dt} = k_{hyd,i}X_i \tag{7}$$

where S_j is the product of hydrolysis, i.e. soluble sugars, amino acids and LCFAs from X_i, i.e. carbohydrates, proteins, and lipids, respectively.

The Monod equation (Equation (8)) is used to represent the growth of biomass on each of these soluble substrates.

$$\frac{dX_j}{dt} = Y_j k_{m,j}\frac{S_j}{K_{S,j}+S_j}X_j I_{pH}I_{IN,lim} \tag{8}$$

where Y_j is the yield of biomass on a substrate, I_{pH} is the pH inhibition (0.992) and $I_{IN,lim}$ is the nitrogen limitation inhibition (0.998) and $k_{m,j}$ is the maximum specific growth rate. The values of biomass yield from the substrates (Y_j), the hydrolysis constants ($k_{hyd,i}$), half-saturation value ($K_{S,j}$), and Monod maximum specific growth rate ($k_{m,j}$) are taken from Rosen & Jeppsson (2006) and are tabulated in Table A1 in the Appendix. For further details on ADM1 and its implementation the reader is referred to Batstone *et al.* (2002) and Rosen & Jeppsson (2006), respectively. The initial concentration of

carbohydrates, lipids, and proteins are taken as 19.5 g/L, 45.1 g/l, and 8.1 g/L, respectively.

Since the sludge compressibility is very low, the pressure-based solver SIMPLE (Semi-Implicit Method for Pressure Linked Equations) is selected. Momentum, turbulent kinetic energy, turbulence dissipation, and all UDS scalar variables are discretized using a first-order upwind method while the pressure is discretized using the standard method. A computer cluster of $4 \times$ AMD Opteron 6380 2.5 GHz (16 cores) is used for the simulation.

RESULTS

CFD hydrodynamics model

Figure 2(a) shows the contour plot of velocity along the vertical plane. The figure indicates that only sludge near the impeller is moving at significant velocity, whereas inlet velocity does not produce significant velocity compared to the velocity produced by the impeller, and hence its impact on AD mixing is insignificant. The velocity produced by the top and bottom impellers shows a significant difference even though both impellers rotate at the same mixing speed. The reason behind this is explained next, together with the velocity vector shown in Figure 2(b).

Figure 2(b) shows that the velocity vectors produced by the top and bottom impellers point in opposite directions. Hence, the sum of the top and bottom impellers' velocity produces a relative velocity which cancels each other, defeating the purpose of having two impellers, and resulting in low-velocity distribution in the vicinity of the top impeller. Furthermore, this makes a design based on two axial flow impellers in the same axis questionable, and a combination of an axial and radial impeller would make more sense.
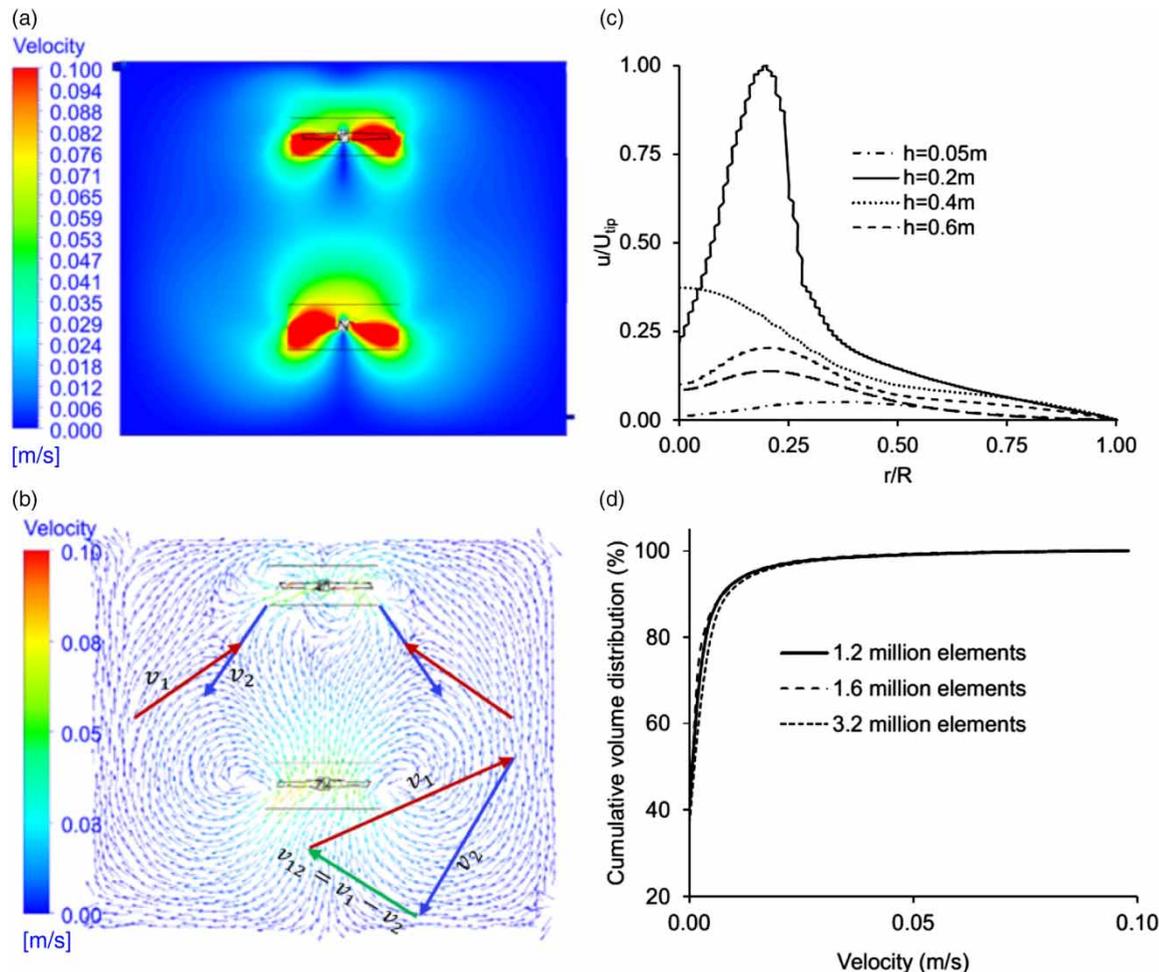

Figure 2 | AD mixing velocity distribution: (a) velocity contour, (b) velocity vector, (c) velocity variation along r/R and digester height (bottom to top), and (d) cumulative volume distribution of velocity and mesh independence test.

In addition to the velocity contour and velocity vector plot, non-dimensional velocity u to the maximum velocity at the tip of the impeller, U_{tip}, i.e. U/U_{tip} along r/R at different height of the digester, is plotted in Figure 2(c). The figure indicates U/U_{tip} approaches 1 near the tip of the impellers and approaches 0 near the center and wall of the digester. The variation of U/U_{tip} indicates that velocity dissipates quickly due to high sludge viscosity as it moves away from the impeller tip.

The cumulative volume distribution of velocity elegantly summarizes the 3-D velocity distribution (Figure 2(d)). The figure quantifies that velocity distribution across the digester volume is not uniform. For example, about 75% of digester volume has a velocity of <5% of maximum velocity, which indicates that the velocity variation between the tip of the impeller and the rest of the digester volume is very high.

Mesh independence of the simulation is analyzed based on the mass balance between the inlet and outlet of the digester and the evaluation of cumulative velocity distribution variation with mesh size (Figure 2(d)). A closed mass balance is attained in all cases, and variation of velocity distribution in an anaerobic digester volume is not significant as such. For example, the cumulative velocity distribution variation between 1.6 million and 3.2 million elements is less than 7%.

Advanced CFD–kinetics modelling: a comparison of advection and advection–diffusion transport

Concentration distribution contour plot

Figures 3 and 4 show contour plots of soluble sugar concentration and biomass distribution variation under advection and different advection–diffusion transport. This is further clarified by the Pe variation tabulated in Table 1. The table indicates that Pe varies along r/R and height (bottom to top) of the digester. Regions around the top, bottom, near the corners, and walls of the digester have a Pe < 1, which means diffusion transport is dominant in these regions. The remaining regions have a Pe > 1 meaning that advection transport is dominant.

Figures 3(a) and 4(a) indicate the contour plots of soluble sugar and biomass concentration under advection transport (Equation (2)). Here, the concentration of soluble sugar and biomass varies widely between the regions with Pe > 1 and Pe < 1. The maximum concentrations of soluble sugar and biomass are ≥ 39 g/m³ and ≥ 3.6 g/m³, respectively, in a region with Pe < 1, and the corresponding minimum concentrations are ≤ 30 g/m³ and ≤ 2.4 g/m³, respectively, in a region with Pe > 1. Due to the high concentration of soluble sugar and biomass near the corners
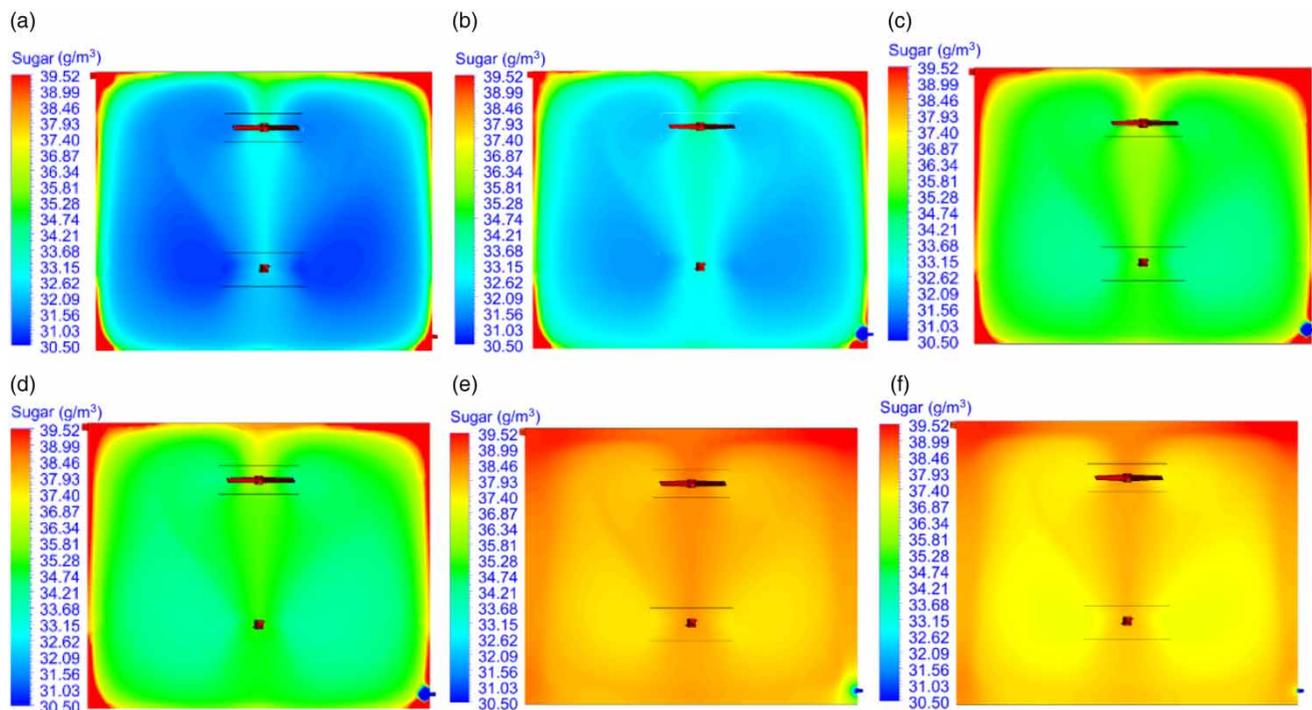

Figure 3 | Contour plot of soluble sugar concentration distribution in AD under (a) advection, (b) advection–molecular diffusion transport, (c)–(e) advection–turbulent diffusion transport, $Sc_t = 0.9$, 0.7, and 0.5, respectively, and (f) advection–(molecular and turbulent) diffusion transport, $Sc_t = 0.9$.

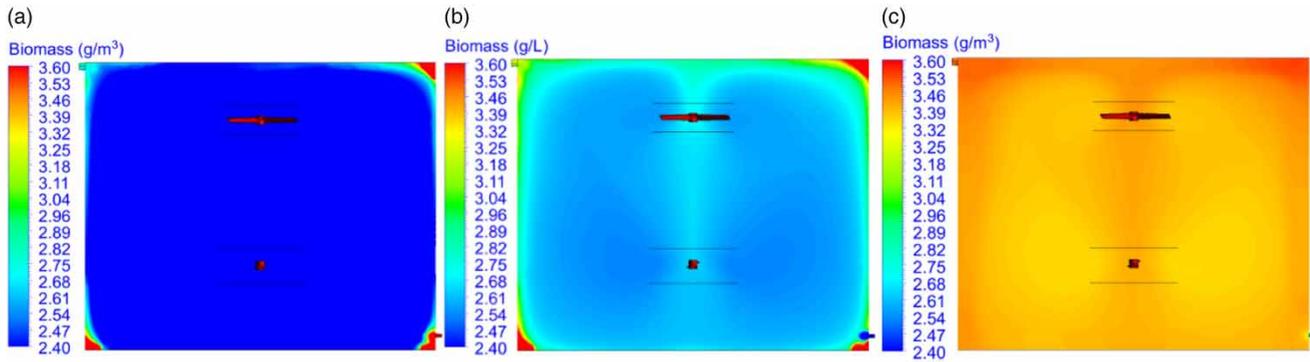**Figure 4** | Contour plot of biomass distribution in a vertical plane under (a) advection transport diffusion (b) advection–molecular diffusion transport (c) advection–(molecular and turbulent) diffusion transport with $Sc_t = 0.7$.

Table 1 | Variation of Peclet number along r/R and height (from bottom to top)

and walls, the soluble sugar and biomass concentration distributions in a region with Pe > 1 are low, hence indicating poor mixing uniformity.

Figures 3(b) and 4(b) show the distribution of soluble sugar and biomass under advection–molecular diffusion transport, respectively. In this case, the homogeneity of soluble sugar and biomass concentration in a region with Pe > 1 increases because of molecular diffusion from a region with Pe < 1 to a region with Pe > 1. The lowest soluble sugar and biomass concentration, distribution along the plane in Figures 3(b) and 4(b) changed to 33 g/m³ and 2.7 g/m³, respectively, under advection–molecular diffusion transport, corresponding to ≤ 30 g/m³ and ≤ 2.7 g/m³ under sole advection transport. The highest concentration near the corner with Pe < 1 is still ≥ 39 g/m³ and ≥ 3.6 g/m³ under advection–molecular diffusion transport.

The impact of mixing due to advection–turbulence diffusion is shown in Figure 3(c)–3(e) for different Sc_t. Under advection–turbulent diffusion, the uniformity of soluble sugar concentration is much higher compared to the advection and advection–molecular diffusion transport. The concentration distribution for $Sc_t = 0.9$ and 0.7 is almost similar. The lowest concentration of soluble sugar is about 35 g/m³ for $Sc_t = 0.9$ and 0.7, while it is about 37 g/m³ for $Sc_t = 0.5$. Uniformity of soluble sugar increases with decreasing Sc_t, and this indicates that turbulent mixing efficiency increases when turbulent eddy diffusivity is dominating turbulent viscosity (Equation (5)).

In the advection–(molecular and turbulent) diffusion transport model (Figures 3(f) and 4(c)), the homogeneity of both soluble sugar and biomass concentrations was found to be higher than all cases discussed. Unlike other models, in advection–(molecular and turbulent) diffusion transport, the ranges of minimum and maximum concentration distribution in a region with Pe > 1 and Pe < 1 are much more comparable. For example, the minimum and maximum concentrations of soluble sugar are about 37 g/m³ and 39 g/m³, respectively. Since both molecular and turbulent diffusion always exist together, it is recommended to model combined advection–diffusion (molecular and turbulent) to describe AD mixing homogeneity accurately. The contour plot and cumulative volume distribution discussed did not include the results of soluble amino acids, LCFAs, and their corresponding biomass because their concentration distribution patterns are similar to soluble sugar and biomass.

Non-dimensional concentration variation along the radius and height

In a similar approach to non-dimensional velocity distribution shown in Figure 2(b), the non-dimensional concentration distribution of soluble sugar is plotted along r/R at different heights of the digester for advection and advection–diffusion transport models (Figure 5). Soluble sugar concentration is non-dimensionalized by dividing the concentration of soluble sugar (C) along r/R
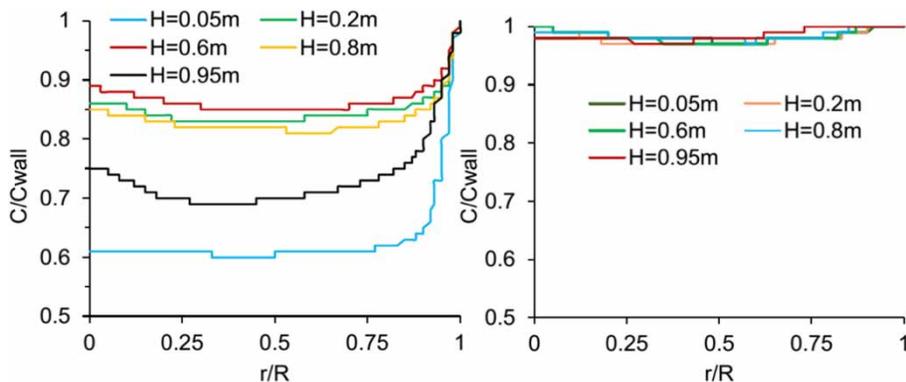
Figure 5 | Non-dimensional plot of soluble sugar concentration along r/R at different digester height: advection transport (left) and advection–diffusion transport (right).

by the maximum concentration of the soluble sugar (C_{wall}) at the wall. The ratio of C and C_{wall} (C/C_{wall}) along r/R at different height of the digester ranges between 0.6 and 1 ($0.6 \leq C/C_{wall} \leq 1$) for the advection transport model (Figure 5 left).

Figure 5 (right) shows C/C_{wall} is between 0.96 and 1 ($0.96 < C/C_{wall} \leq 1$) at all indicated heights, indicating the digester is nearly ideally mixed under advection–diffusion transport. Unlike non-dimensional velocity distribution, U/U_{tip} (Figure 2(c)), non-dimensional concentration distribution, C/C_{wall} (Figure 5), along r/R is uniform. So, making conclusions about AD mixing homogeneity based on velocity and concentration distribution leads to very different outcomes.

Mixing uniformity analysis using cumulative volume distribution

In addition to concentration distribution contour plots and a non-dimensional plot along r/R and height (Figures 2–5) in 2-D, additional information can be extracted by plotting a concentration distribution derived from the 3-D volume.

A comparison is provided for soluble substrates and biomass sole advection transport as well as all advection–diffusion transport cases modelled. Distributions of soluble sugar and biomass shift to the right for all advection–diffusion transport cases compared to the advection-only transport model. The shaded area under the curve indicates the increase in the uniformity of AD mixing by advection–diffusion for that case. For example, the shaded area in Figures 6(a) and 7(a) shows a change of soluble sugar and biomass concentration distribution, respectively, for advection–molecular diffusion, and the shaded area is small. A small shaded area means the difference of soluble substrates

and biomass distribution under advection–molecular and sole advection transport is rather small. Mainly, it is minimal for biomass distribution due to the small molecular diffusion coefficient of biomass (Figure 7(a)).

Figure 6(b)–6(d) show the effect of advection–turbulent diffusion transport for different Sc_t. The figures indicate that the shaded area increases with decreasing the Sc_t, which means mixing performance increases when eddy mass diffusivity dominates turbulent diffusion (Equation (5)). The shaded area under advection–turbulent diffusion transport is larger than under advection–molecular diffusion transport. The shaded area is almost the same for a model with $Sc_t = 0.7$ and $Sc_t = 0.9$, and the largest for a model with $Sc_t = 0.5$.

In advection–(molecular and turbulent) diffusion transport, the homogeneity of mixing increased much more compared to the rest of the advection–diffusion transport cases considered (Figures 6(e) and 7(b)) except advection–turbulent diffusion with $Sc_t = 0.5$. The shaded area comparison of advection–molecular diffusion, advection–turbulent diffusion, and advection–(molecular and turbulent) diffusion transport shows that advection–diffusion yields a higher homogeneity of AD.

Generally, the steeper the slope of the cumulative volume distribution, the better the homogeneity of AD. In other words, change in concentration distribution variation is smaller, with change in cumulative volume distribution at the steepest slope.

DISCUSSION

In the conventional CFD hydrodynamics model, the uniformity of mixing comparison is based on relative velocity distribution (Figure 2), i.e. a high-velocity region near the impeller tip is taken as a well-mixed region, which is used
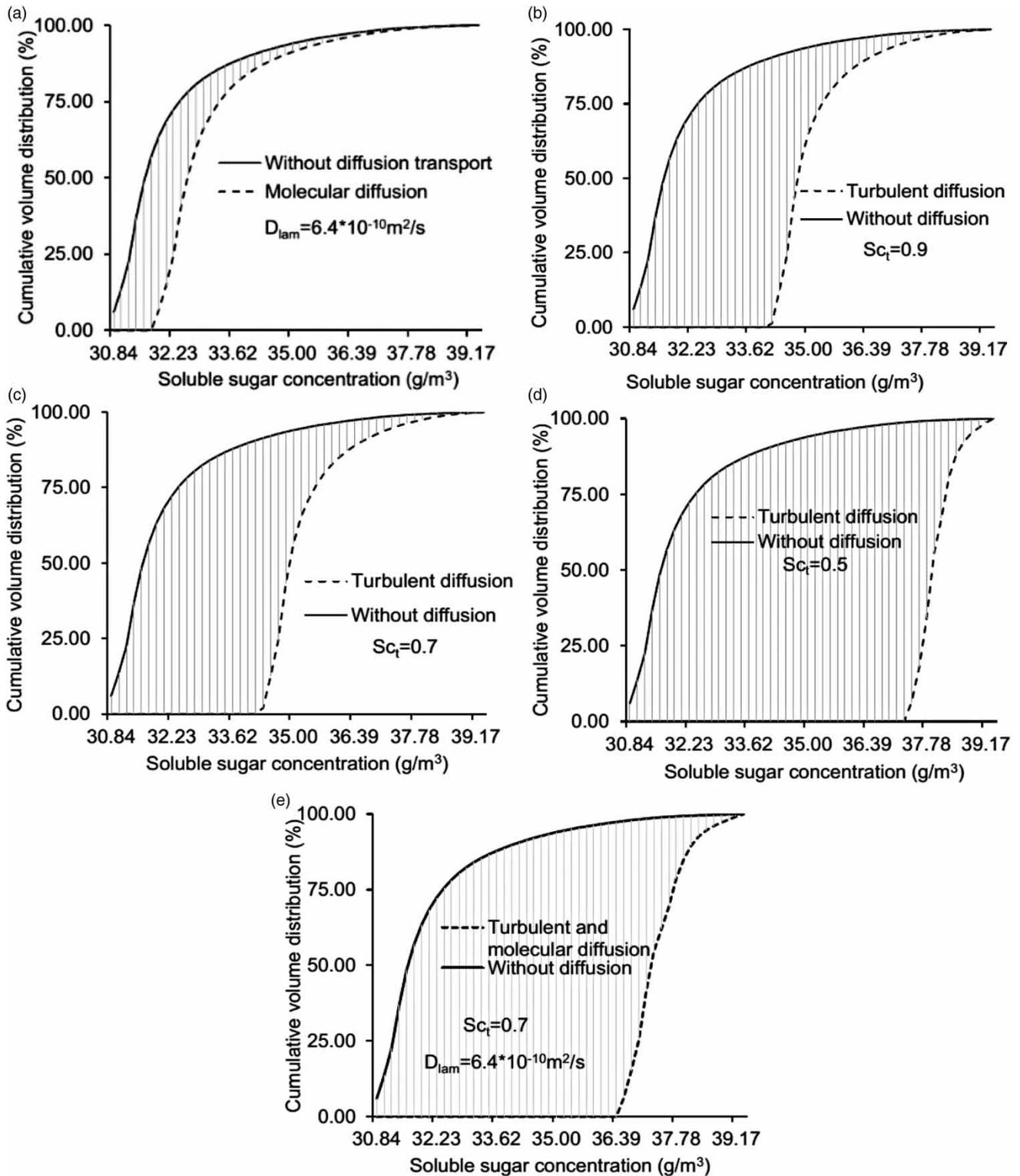
Figure 6 │ Cumulative volume distribution of soluble sugar concentration: comparison of sole advection transport with (a) molecular diffusion, (b) turbulent diffusion, $Sc_t = 0.9$, (c) turbulent diffusion, $Sc_t = 0.7$, (d) turbulent diffusion, $Sc_t = 0.5$, (e) molecular and turbulent diffusion transport, $Sc_t = 0.7$.

as a reference point to compare the remaining velocity distribution in an anaerobic digester. The analysis of velocity distribution leads to the conclusion that the lowest velocity region relative to the velocity near the impeller tip is
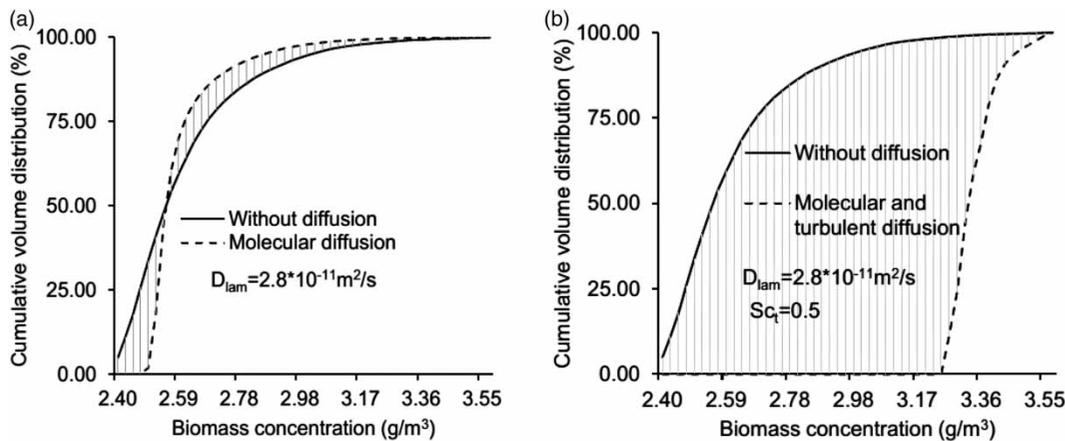
Figure 7 | Biomass concentration cumulative distribution sensitivity analysis: a comparison of advection (without diffusion) transport with (a) molecular diffusion, and (b) molecular and turbulent diffusion transport, Sct = 0.7.

assumed as not mixed well irrespective of mixing due to turbulence and molecular diffusion. So, making conclusions about the homogeneity of AD in terms of relative velocity distribution analysis is tricky and can lead to inaccurate conclusions. Because the minimum velocity required to produce homogeneity is not known and the conventional CFD model ignores the contribution of (molecular and turbulence) diffusion.

In the advanced advection–diffusion transport model, the limitations of the conventional CFD model mixing description improved in two ways. First, the homogeneity of mixing is described based on concentration distribution. Second, the effects of mixing due to diffusion transport are included. Describing the homogeneity of AD based on concentration distribution, including the effect of diffusion transport on AD mixing, gives more comprehensive information.

The results of different advection–diffusion transport model cases shown in the contour plot (Figures 3 and 4) and cumulative volume distribution (Figures 6 and 7) shows that changing the diffusion transport variables affects the homogeneity of soluble substrates and biomass. The models indicate that soluble substrates and biomass are less homogeneous under the sole advection transport, and the homogeneity of soluble substrates and biomass increases under advection–diffusion transport.

The cumulative volume distribution under advection–diffusion transport (Figures 6(f) and 7(b)) indicate that the variation of concentration distribution is minimal, and it is close to a homogeneously mixed AD. This shows that the effect of diffusion transport is significant in the homogenization of AD and should be considered in AD mixing optimization. Since molecular diffusion is a material property and mixing optimization cannot improve it,

considering turbulence generation techniques in anaerobic digester and mixer design increases the homogeneity of substrates and biomass distribution.

In general, CFD hydrodynamics and advection–diffusion transport give significantly different results. Velocity is a carrier/transporter of scalar variables like substrates and biomass, and it is not a good mixing descriptor by itself. So, explaining the homogeneity of AD based on concentration improves the interpretation of AD mixing, including the impact of diffusion transport.

CONCLUSION

Conventional CFD hydrodynamics models solely based on the velocity description fall short of describing the homogeneity of AD mixing. Advanced CFD modelling, including advection–diffusion transport, improves AD mixing description and understanding. Mixing seems to be more profound based on concentration profiles than what would be expected from velocity distributions. Analyzing the homogeneity of AD mixing in terms of concentration significantly facilitates the interpretation of the computed results. As the contribution of (molecular and turbulent) diffusion transport is significant, it should be included in future mixing optimization studies.

ACKNOWLEDGEMENTS

SUPPLEMENTARY MATERIAL

The Supplementary Material for this paper is available online at https://dx.doi.org/10.2166/wst.2020.076.

REFERENCES

Ansys 2009 *Ansys Fluent 12. Theory Guide*. Ansys, Canonsburg, PA, USA.

Batstone, D., Keller, J., Angelidaki, I., Kalyuzhnyi, S., Pavlostathis, S., Rozzi, A. & Vavilin, V. 2002 The IWA anaerobic digestion model No. 1(ADM1). *Water Science and Technology* **45** (1), 65–73. https://doi.org/10.2166/wst.2008.678.

Bridgeman, J. 2012 Computational fluid dynamics modelling of sewage sludge mixing in an anaerobic digester. *Advances in Engineering Software* **44** (1), 54–62. https://doi.org/10.1016/j.advengsoft.2011.05.037.

Conti, F., Wiedemann, L., Sonnleitner, M., Saidi, A. & Goldbrunner, M. 2019 Monitoring the mixing of an artificial model substrate in a scale-down laboratory digester. *Renewable Energy* **132**, 351–362. https://doi.org/10.1016/j.renene.2018.08.013.

Craig, K. J., Nieuwoudt, M. N. & Niemand, L. J. 2013 CFD simulation of anaerobic digester with variable sewage sludge rheology. *Water Research* **47** (13), 4485–4497. https://doi.org/10.1016/j.watres.2013.05.011.

Donoso-Bravo, A., Sadino-Riquelme, C., Gómez, D., Segura, C., Valdebenito, E. & Hansen, F. 2018 Modelling of an anaerobic plug-flow reactor. Process analysis and evaluation approaches with non-ideal mixing considerations. *Bioresource Technology* **260**, 95–104. https://doi.org/10.1016/j.biortech.2018.03.082.

Douarche, C., Buguin, A., Salman, H. & Libchaber, A. 2009 *E. coli* and oxygen: a motility transition. *Physical Review Letters* **102** (19), 198101. https://doi.org/10.1103/PhysRevLett.102.198101.

Gaden, D. L. F. & Bibeau, E. L. 2013 A general three-dimensional extension to ADM1: the importance of an integrated fluid flow model. *IWA/WEF Wastewater Treatment Seminar* **4**, 318–321.

Ghatak, H. R. 2016 Nonideal flow in reactors. In: *Reaction Engineering Principles*, 1st edn. CRC Press, Boca Raton, FL, USA, pp. 260–285. https://doi.org/10.1201/9781315367781-8.

Leonzio, G. 2018 Study of mixing systems and geometric configurations for anaerobic digesters using CFD analysis. *Renewable Energy* **123**, 578–589. https://doi.org/10.1016/j.renene.2018.02.071.

Meroney, R. N. & Colorado, P. E. 2009 CFD simulation of mechanical draft tube mixing in anaerobic digester tanks. *Water Research* **43** (4), 1040–1050. https://doi.org/10.1016/j.watres.2008.11.035.

Øyaas, J., Storrø, I., Svendsen, H. & Levine, D. W. 1995 The effective diffusion coefficient and the distribution constant for small molecules in calcium-alginate gel beads. *Biotechnology and Bioengineering* **47** (4), 492–500. https://doi.org/10.1002/bit.260470411.

Rezavand, M., Winkler, D., Sappl, J., Seiler, L., Meister, M. & Rauch, W. 2019 A fully Lagrangian computational model for the integration of mixing and biochemical reactions in anaerobic digestion. *Computers and Fluids* **181**, 224–235. https://doi.org/10.1016/j.compfluid.2019.01.024.

Rosen, C. & Jeppsson, U. 2006 *Aspects on ADM1 Implementation within the BSM2 Framework*. Lund University, Lund, Sweden.

Tominaga, Y. & Stathopoulos, T. 2007 Turbulent Schmidt numbers for CFD analysis with various types of flowfield. *Atmospheric Environment* **41** (37), 8091–8099. https://doi.org/10.1016/j.atmosenv.2007.06.054.

Wiedemann, L., Conti, F., Saidi, A., Sonnleitner, M. & Goldbrunner, M. 2018 Modeling mixing in anaerobic digesters with computational fluid dynamics validated by experiments. *Chemical Engineering and Technology* **41** (11), 2101–2110. https://doi.org/10.1002/ceat.201800083.

Wu, B. 2010 Computational fluid dynamics investigation of turbulence models for non-Newtonian fluid flow in anaerobic digesters. *Environmental Science and Technology* **44** (23), 8989–8995. https://doi.org/10.1021/es1010016.

Wu, B. 2012 Integration of mixing, heat transfer, and biochemical reaction kinetics in anaerobic methane fermentation. *Biotechnology and Bioengineering* **109** (11), 2864–2874. https://doi.org/10.1002/bit.24551.

Wu, B. & Chen, S. 2008 CFD simulation of non-Newtonian fluid flow in anaerobic digesters. *Biotechnology and Bioengineering* **99** (3), 700–711. https://doi.org/10.1002/bit.21613.

Yu, L., Ma, J. & Chen, S. 2011 Numerical simulation of mechanical mixing in high solid anaerobic digester. *Bioresource Technology* **102** (2), 1012–1018. https://doi.org/10.1016/j.biortech.2010.09.079.